9. Nair, M. K., Koshy, P. K., Jacob, P. M., Rao, E. V. V. B., Nampoothiri, K. U. K. and Iyer, R. D., A root (wilt) resistant coconut hybrid and strategy for resistance breeding. *Indian Coconut J.*, 1996, **27**, 2–5.
10. Solomon, J. J., Sasikala, M. and Shanta, P., A serological test for the detection of root (wilt) disease of coconut. In *Coconut Research and Development* (ed. Nayar, N. M.), Wiley Eastern Ltd, New Delhi, 1983, pp. 401–405.
11. Allen, O. N., In *Experiments in Soil Bacteriology*, 1959, 3rd edn, p. 117.
12. Martin, J. P., Use of acid, rose bengal and streptomycin in the plate method for estimating soil fungi. *Soil Sci.*, 1950, **69**, 215–232.
13. Becking, J. H., Nitrogen fixing bacteria of genus *Beijerinckia* in South African soils. *Plant Soil*, 1959, **11**, 193–206.
14. Pikovskaya, R. I., Mobilization of phosphorus in soil in connection with vital activity of some soil microbial species. *Mikrobiologiya*, 1948, **17**, 362–370.
15. Hankin, L. and Anagnostakis, S. L., Solid media containing carboxymethyl-cellulose to detect $C_X$ cellulase activity of microorganisms. *J. Gen. Microbiol.*, 1977, **98**, 109–115.
16. Bunt, J. S. and Rovira, A. D., Microbiological studies of some subantartic soils. *J. Soil Sci.*, 1955, **6**, 119–128.
17. Potty, V. P., George, M. and Jayasankar, N. P., Effect of crop mixing on coconut rhizosphere. *Indian Coconut J.*, 1977, **8**, 1–2.
18. Alice, E. J., Karunakaran, P. and Samraj, J., A comparative study of the rhizosphere microflora of coconut palms from diseased and healthy areas with reference to root (wilt). *Indian Coconut J.*, 1980, **11**, 1–4.
19. Gopal, Murali, Gupta, Alka, Nair, C. P. R. and Rajan, P., Effect of systemic soil insecticides and plant product on microbial load of soil in root (wilt) affected coconut monocropping ecosystem. *Coconut Res. Dev.*, 2001, **17**, 52–71.
20. Nagaraj, A. N. and Menon, K. P. V., Observation on root decay in coconuts, its cause and its relation to the foliar symptoms of disease in the disease belt of Travancore–Cochin. *Indian Coconut J.*, 1955, **8**, 97–105.
21. Maramorosch, K., A survey of coconut disease of uncertain etiology. Report FAO, UN, Rome, 1964, p. 39.
22. Joseph, T. and Jayasankar, N. P., Evaluation of root degeneration in coconut in relation to root (wilt) disease. *Plant Dis.*, 1981, **66**, 666–669.
23. Anon., Annual Report 1997, Central Plantation Crops Research Institute, Kasaragod, 1997, p. 45.
24. Verghese, E. J., Sankaranarayanan, M. P. and Menon, K. P. V., Chemical studies on the leaf and root (wilt) disease of coconut in Travancore–Cochin. II. Nutrient contents of leaves of healthy and diseased palms. In Proc. First. Conf. Coconut Research Workers, Trivandrum, 1959, pp. 18–23.
25. Menon, K. P. V. and Pandalai, K. M., In *The Coconut Palm – A Monograph*, Indian Central Coconut Committee, Ernakulam, 1958, p. 394.
26. Pillai, T. N. V., Silica content in coconut (*Cocos nucifera*) kernel and water. *Curr. Sci.*, 1967, **24**, 667–668.
27. Jones, L. H. P. and Handrecht, K. A., Silica in soils, plants, and animals. *Adv. Agron.*, 1967, **19**, 107–149.
28. Vandevivere, P., Welch, S. A., Ullman, W. J. and Kirchman, D. L., Enhanced dissolution of silicate minerals by bacteria at near-neutral pH. *Microbial Ecol.*, 1994, **27**, 241–251.
29. Dwivedi, R. S., Mathew, C., Michael, K. L., Ray, P. K. and Amma, B. S. K., Carbonic anhydrase, carbon assimilation and canopy structure in relation to nut yield of coconut. Indian Natl. Sci. Acad. Symp. on Photosynthesis and Productivity, Lucknow, 1978, pp. 44–46.
30. Epstein, E., Silicon. *Annu. Rev. Plant Physiol. Plant Mol. Biol.*, 1999, **50**, 641–664.
31. Rajagopal, V., Patil, K. D. and Amma, B. S. K., Abnormal stomatal opening in coconut palms affected with root (wilt) disease. *J. Exp. Bot.*, 1986, **37**, 1398–1405.
32. Rajagopal, V., Amma, B. S. K. and Patil, K. D., Water relations of coconut palms affected with root (wilt) disease. *New Phytol.*, 1987, **105**, 289–293.
33. Joseph, K. V. and Jayasankar, N. P., Polyphenol content in coconut roots in relation to root (wilt) disease. *J. Plant. Crops*, 1973, **1**, 99–101.
34. Watteau, F., Villemin, G., Mansot, J. L., Ghanbaja, J. and Tontain F., Localization and characterization by Electron Energy Loss Spectroscopy (EELS) of the brown cellular substances of beech roots. *Soil Biol. Biochem.*, 1996, **28**, 1327–1332.
35. Belanger, R. R., Bowen, P. A., Ehret, D. L. and Menzies, J. G., Soluble silicon. Its role in crop and disease management of greenhouse crops. *Plant Dis.*, 1995, **79**, 329–336.

ACKNOWLEDGEMENTS. We are grateful to Dr J. J. Solomon, Retd Head, CPCRI, Kayangulam and the anonymous referees for critically going through the manuscript and making valuable suggestions.

Received 13 November 2004; revised accepted 19 August 2005

# IWAVE: an ocean simulation model for internal waves

**G. V. Krishna Kumar* and P. Balasubramanian**

Naval Physical and Oceanographic Laboratory, Thrikkakara, Kochi 682 021, India

**Effective usage of scarce resources (ships, instruments, etc.) requires a coherent and rational approach to develop any underwater system. One of the important tasks towards achieving this is to simulate the performance of the proposed system under all oceanic conditions before it is being developed. Internal waves (IWs) play a major role in ocean thermodynamics, underwater acoustic transmission, etc. In order to understand the behaviour of IWs and their role in various physical processes in the ocean, we have developed an IW model, IWAVE based on the Garrett–Munk modal spectrum. In this communication we present detailed implementation procedures of the model and also a technique to solve the eigenvalue problem accurately. An algorithm based on central finite difference and QR techniques was implemented to find the eigen-wavenumbers and modes (dispersion relations). IWAVE simulates temperature and salinity (estimated sound speed also) structure due to IWs in the ocean. Experiments were conducted to validate the model off the west coast of India. Variances of the measured and simulated sound speed are in good agreement.**

**Keywords:** Dispersion relation, GM model, internal waves, simulation, validation.

IN a stratified medium, a fluid parcel displaced from its equilibrium level experiences a restoring force propor-

*For correspondence. (e-mail: garimella70@yahoo.com)

tional to reduced gravity and the disturbance propagates in the form of an internal wave (IW). IWs are a ubiquitous feature in both deep and shallow waters. They induce vertical motions in the water column, which changes the temperature and salinity (sound speed) at a fixed depth and the variations are proportional to the energy of the IW as well as the density gradient. This has significant impact on the underwater acoustic transmission. Efforts to quantify and predict the impact of IWs on acoustic transmission have been made by several authors over the last few decades[1–5]. In the recent past some studies were done on IWs in the seas around India, utilizing the time series measurements from stationary ships and from moored oceanographic buoys. However, these measurements cannot give a true frozen field of the IWs to accurately estimate the effect of these waves on acoustic transmission. Due to the lack of understanding of the physical processes associated with IWs, a true dynamical model of the oceanic IWs is not currently possible. Thus the effect of the IW field on acoustic propagation has to be predicted using statistical simulations of probable IW characteristics. Hence we have developed an IW simulation model (IWAE) to study the impact. Often the sonar operator has little or no information (data) about the prevailing environment; the model was developed keeping this in view. IWAVE simulates a background IW field and calculates the resulting sound speed structure as a function of range, depth and time and makes no attempt to simulate internal solitons or other oceanographic features.

Using the equations of momentum and continuity in a stratified ocean, under certain assumptions (incompressible, no horizontal density gradient, small or no mean shear and horizontal isotropy), a modal solution for IWs can be derived. The exact dispersion relation for the IWs in the density stratified rotated ocean is a solution of the eigenvalues problem give by Gill[6]:

$$\frac{\mathrm{d}^2 W_{\omega,j}(z)}{\mathrm{d}z^2} + k^2\left[\frac{N^2(z)-\omega^2}{\omega^2 - f^2}\right] W_{\omega,j}(z) = 0, \qquad 0 \le z \le H, \tag{1}$$

where $H$ is the depth of the water column (range-independent, i.e. flat or slowly varying), $\omega$ is the IW frequency (i.e. frequency at which solutions are sought), $f$ is the inertial frequency which depends on the rotation rate of the earth (angular frequency $\Omega$) and the latitude $\varphi$ ($f = 2\Omega\sin\varphi$), and $N$ is buoyancy frequency (depth-dependent), defined by

$$N(z) = \left(-\frac{g}{\bar{\rho}}\frac{\mathrm{d}\rho}{\mathrm{d}z}\right)^{1/2}, \tag{2}$$

where $g$ is the gravitational acceleration and $\bar{\rho}$ the mean density of the medium. IW frequencies $\omega$ are limited to the range between inertial frequency $f$ at the lower end and maximum buoyancy frequency $N_{\max}$ at the higher end. Solving this equation using the boundary conditions $W_{\omega,j}(0) = W_{\omega,j}(H) = 0$ provides the modes of the system. These modes oscillate only in the region of the water column, where the IW frequency $\omega$ is smaller than the buoyancy frequency $N(z)$. Outside this region the solutions are evanescent (i.e. exponentially decreasing). Each frequency $\omega$ has its own set of depth-dependent vertical modes $W_{\omega,j}(z)$, where $j$ indicates the number of the mode. Therefore, the vertical displacement of the linear IW field can be expressed as a combination of plane waves as a weighted double sum over mode number $j$ and frequency $\omega$ of the form:

$$\xi(x,z,t) = \int_f^N \sum_{j=1}^{j_{\max}} A(\omega, j) W_{\omega,j}(z) \mathrm{e}^{i[k_{\omega,j}x - \omega t + \psi]} \mathrm{d}\omega, \tag{3}$$

where $A(\omega, j)$ is the $j$th mode amplitude associated with the Garrett–Munk (GM) spectrum, $k_{\omega j}$ is the corresponding wave number, $x$ is the range, $t$ the time and $\psi$ is the phase. $A(\omega, j)$ is a zero mean Gaussian random variable weighted with the GM spectrum described below.

In a series of publications during the 1970s, Garrett and Munk have formulated an empirical model of the IW modal spectrum based on experimental observations[7–9]. The GM model incorporates more observational data than any other model and has also been widely accepted by the scientific community worldwide. The following assumptions were made either explicitly or implicitly in the derivation of the GM model, i.e. linear, no mean shear, flat (or slowly varying bottom), horizontally homogeneous (or slowly varying) density field and a random IW field. The GM spectrum is based on a distribution of energy over modes and frequencies. The distribution of energy over modes (discrete) and the distribution of energy over frequency (continuous) are independent of each other. The resulting energy is the product of these two terms and an overall energy parameter.

$A(\omega, j)$ in eq. (3) is expressed in terms of the GM spectrum[2]:

$$A(\omega, j) = \left[2rB(\omega)H(j)\int_0^H N(z)\,\mathrm{d}z\right]^{1/2}, \tag{4}$$

where $r$ (320 $\mathrm{m}^2$ cph is suggested for deep waters) is an energy parameter which depends upon season and location. The GM model assumes that the distribution of energy over modes is based on an infinite number of modes. However, eq. (1) can be solved for a finite number of modes only. Also experimental results have confirmed that the first few modes account for 98% of the total energy. Therefore, using finite number of modes without any

modification to the GM model will ignore the energy in the higher order modes. Hence the parameters $B(\omega)$ and $H(j)$ of the GM model are modified accordingly[10] and are given by:

$$B(\omega) = \frac{2f}{\pi\omega\sqrt{\omega^2 - f^2}}, \qquad \int_f^{N_{\max}} B(\omega)\, d\omega = 1, \tag{5}$$

$$H(j) = \frac{(j^2 + j_*^2)^{-\frac{P}{2}}}{\sum_{j=1}^{M} (j^2 + j_*^2)^{-\frac{P}{2}}}, \qquad \sum_{j=1}^{M} H_M(j) = 1. \tag{6}$$

$M$ and $H_M(j)$ are introduced to indicate the finite number of modes. If few modes are used, the relative energy distribution between the lower order modes changes significantly. To correct for this effect, the modal bandwidth parameter $j_*$ is chosen[10] to depend on the number of modes $M$.

$$j_* = \begin{cases} 1 \text{ for } M \le 2 \\ 2 \text{ for } M = 3 \\ 3 \text{ for } M \ge 4. \end{cases} \tag{7}$$

$j_*$ has the effect of increasing the proportion of energy in the lowest mode(s) when $M$ is small. This ensures that the relative energy distribution between the first few modes changes only little. $P$ is called the modal slope parameter and a value of 2 is used in our model.

The vertical displacement $\xi(x, z, t)$ given by eq. (3) is modified by a sum over a finite number of modes and frequencies. We define a finite (fifteen frequencies) set of frequencies between the inertial frequency $f$ and the maximum buoyancy frequency $N_{\max}$. These frequencies are chosen equally distributed on a logarithmic scale. For each frequency eq. (1) is solved for a number of $M$ modes. Modes are denoted by $W_{\omega,j}(z)$. The maximum number of modes depends on the depth $H$ of the water column. Therefore, we choose $M$, the maximum number of modes suggested in the Elliot and Jackson[11], as

$$M = \begin{cases} 2 \text{ for } 0 < H < 25 \text{ m} \\ 3 \text{ for } 25 \le H < 100 \text{ m} \\ 4 \text{ for } 100 \le H < 250 \text{ m} \\ 5 \text{ for } H \ge 250 \text{ m}. \end{cases} \tag{8}$$

The above mentioned scheme assumes that the first few lower order modes account for 98% of the total energy in the shallow waters. However, eqs (7) and (8) may not hold good for all the seasons and sites, but rather work as a guide since the parameters $j_*$, $P$ and the number of modes are site and season-specific. This needs to be checked and calibrated for the Indian Ocean region. Thus knowledge of these parameters at the simulation site improves the reliability of the simulations. The integral over frequencies was approximated by a sum and $e^{i(k_{\omega,j}x - \omega t)}$ approximated by $\sin(k_{\omega,j}x - \omega t)$. Then one can obtain an expression for the vertical displacement as a function of range, depth, and time as:

$$\xi(x, z, t) = \sum_{\omega=f}^{N_{\max}} \sum_{j=1}^{M(\omega)} A(\omega, j) W_{\omega,j}(z) \sin(k_{\omega,j}x - \omega t)\sqrt{\Delta\omega}. \tag{9}$$

The term $\sqrt{\Delta\omega}$ comes from the approximation of the integral by a sum.

A numerical method has been developed for calculating the dispersion relations, which must be satisfied for the free propagation of internal gravity waves. The dispersion relations are required in any simple mathematical treatment of the waves produced by a disturbance in the fluid. Dispersion relations essentially describe how a complex waveform may be developed. These waveforms might be generated by a number of mechanisms and can be expressed mathematically as an infinite sum of basic free waves. Determination of the dispersion relations in any given environment is thus a desirable computational step in the mathematical description of any wave field, which might be expected in that environment. We now describe a numerical procedure to obtain the dispersion relations.

By solving eq. (1), one can obtain the exact dispersion relations of the IW field. In eq. (1) we assumed that the temporal frequency $\omega$ (both frequency and wavenumber are unknown) is known and attempted to find a discrete set of spatial wavenumbers $k$ as eigenvalues for each frequency. The eigenvalues ($k$ is a spatial wavenumber in rad/m) and eigenvectors (modes) depend upon the water depth $H$ (m), buoyancy frequency profile $N(z)$, inertial frequency $f$ (rad/s) and frequency $\omega$ (rad/s). The IW modes $W(z)$ satisfy the eigenvalue problem given by eq. (1) along with the boundary conditions. The IW modes are normalized so that

$$\int_0^H \left( \frac{N^2(z) - \omega^2}{\omega^2 - f^2} \right) W_i(z) W_j(z) dz = \delta_{ij}. \tag{10}$$

The weight function $(N^2(z) - \omega^2/\omega^2 - f^2)$ which multiplies the eigenvalue in eq. (1), can be both positive and negative depending on the buoyancy frequency profile and the frequency at which the equation is being solved. Therefore, conventional methods like shooting (especially in estimation of eigenvectors) can lead to instabilities and failure. Hence an alternative numerical scheme which is robust and reliable has been worked out[12].

A finite difference approximation of the eigenvalue problem in eq. (1) is obtained by dividing the interval $[0, H]$

into $N$ parts of size $\Delta z = H/N$. Equation (1) can be written as:

$$\frac{d^2W(z)}{dz^2} + \lambda b^2(z) W(z) = 0, \qquad 0 \le z \le H, \tag{11}$$

where $W(0) = W(H) = 0$, $b^2(z) = (N^2(z) - \omega^2/\omega^2 - f^2)$, and $\lambda = k^2$. Then by defining $b_n^2 = b^2(n\Delta z)$ and $W_n = W(n\Delta z)$ for $n = 0, N$ and applying three-point central differencing to eq. (11), one can obtain

$$[-W_{n+1} + 2W_n - W_{n-1}] = \lambda \Delta z^2 b_n^2(z) W_n, \quad n = 1,...,N, \tag{12}$$

where $W_0 = W_N = 0$ (boundary conditions). A matrix equation of the form $AW_m = \lambda_m W_m$ is obtained from the eq. (12). Here $\lambda_m$ is the $m$th eigenvalue of $A$, $W_m$ is the $N \times 1$ eigenvector approximating the mode function, and $A$ is the $N \times 3$ non-symmetric tridiagonal matrix. The diagonal entries in the tridiagonal matrix $A$ are $A_{i,i} = (-2/b_i(z)\Delta z^2), i = 1,2,...,n$, while entries in the super-diagonal and subdiagonal are $A_{i,i+1} = (1/b_i(z)\Delta z^2)$, $i = 1,2,...,n-1$, and $A_{i,i-1} = (1/b_i(z)\Delta z^2), i = 1,2,...,n$ respectively.

Matrix $A$ is non-symmetric and also not positive definite. The eigenvalues and eigenvectors are found using the QR technique, which is robust and stable. The eigenvectors on the depth grid are found and normalized using eq. (10) to obtain IW modes.

The numerical procedure for calculating dispersion relations described earlier has been compared with the analytical solutions to check the reliability of the algorithm. Since the constant buoyancy frequency case possesses an analytical solution, stability and accuracy of the above mentioned numerical scheme has been checked against the same. Analytical solution of the eq. (1) with rigid lid approximation for a constant buoyancy frequency is given by:

$$W_{\omega,j}(z) = \sin\left(\frac{n\pi}{D} z\right), n = 1,...N. \tag{13}$$

For a given frequency $\omega$ the dispersion relation gives the eigen-wavenumber $k_{\omega,j}$,

$$k_{\omega,j} = \frac{n\pi}{D}\sqrt{\frac{\omega^2 - f^2}{N^2 - \omega^2}}. \tag{14}$$

Comparisons have been made for internal tide case (0.0805 cph) where buoyancy frequency is 15 cph, inertial frequency is 0.0141 cph and bottom depth is 50 m. Dispersion relations were estimated for the first ten modes. The difference between the analytical and numerical eigen-wavenumber is given in the Table 1. It is apparent from the table that numerically estimated values match well with the analytical ones. The error increases with increase in the mode number; however, the percentage of mismatch for the 10th mode is only 2. Comparisons between analytical and numerical results have been done for the eigenvectors also. It is evident from Figure 1 that the match between analytical and numerical results is excellent. Comparisons at higher frequencies also show an excellent agreement between the analytical and numerical values.

Vertical velocity structure of the IWs can be used to calculate the time dependent sound speed structure at a regular grid ($x$, $z$, $t$) by the particle tracking method suggested by Jackson and Elliott[10], and Elliott and Jackson[11]. Jackson and Elliot[10] have compared different algorithms for estimation of temperature and salinity and concluded that the particle tracking method works well and it can be implemented with relatively simple code than the time-stepping advection model. Hence we have chosen to implement the particle tracking method in our model also. In this method the initial temperature and salinity profiles were represented by a set of equally spaced water particles, which were allowed to move in response to the vertical

**Table 1.** Errors in numerical eigenvalues for internal tidal frequency

| Mode no. | Analytical | Numerical | Error |
|---|---|---|---|
| 1 | 0.1902 | 0.1902 | 0.0000 |
| 2 | 0.3804 | 0.3802 | 0.0002 |
| 3 | 0.5706 | 0.5698 | 0.0008 |
| 4 | 0.7608 | 0.7588 | 0.0020 |
| 5 | 0.9511 | 0.9471 | 0.0040 |
| 6 | 1.1413 | 1.1345 | 0.0068 |
| 7 | 1.3315 | 1.3208 | 0.0107 |
| 8 | 1.5217 | 1.5057 | 0.0160 |
| 9 | 1.7119 | 1.6892 | 0.0227 |
| 10 | 1.9021 | 1.8710 | 0.0311 |

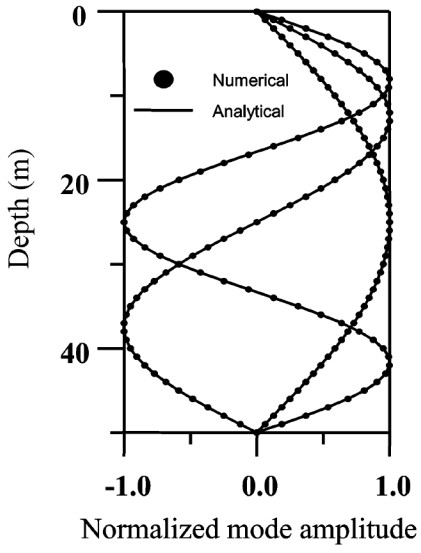


**Figure 1.** Comparison between analytical and numerical solutions for the first three modes at tidal frequency.

velocity field associated with the IW modes. Each particle retained its initial temperature and salinity, and the vertical structure of the water column at a future time was found by interpolating the particle back to the initial grid. The boundary condition as specified above was used at the surface and bottom. The temperature at grid points is obtained by linear interpolation between the particle depths. The resulting temperature values are used to compute the sound speed realizations. However, the disadvantage of this scheme is that particles near the surface (or bottom) may have amplitudes due to high frequency/vertical wavenumber modes, which would cause them to move above the surface (or below the bottom).

One of the requirements for the IW model was that it should need a minimum of input data. As demanded, the model needs a single temperature and salinity profile, an energy level, latitude, and range and timescales for the output sound speed fields. In order to validate the model an experiment was conducted off the west coast of India, in shallow waters, for two days on 7 and 8 May 2002. Two stations were chosen on 7 and 8, where the station depths are ~32 and ~50 m respectively. CTD yo-yo casts were taken for 3 h on 7 May 2002 at 5 min interval and for 1 h 50 min on 8 May 2002 at 5 min interval. Shallow water experiments off Porbandar allow a comparison to be made between the measured and simulated sound speed perturbations due to IWs. We choose to present sound speed profiles rather than temperature and salinity because of their direct utility in sonar range prediction models. Comparisons were done only in the time domain, since we do not have measurements in range. Each time the model has been initialized with the first profile as shown in Figure 2. A total of 36 and 22 profiles are presented in Figure 3 *a* and *b* respectively. In each case the initial sound speed profile has been subtracted from each subsequent profile.

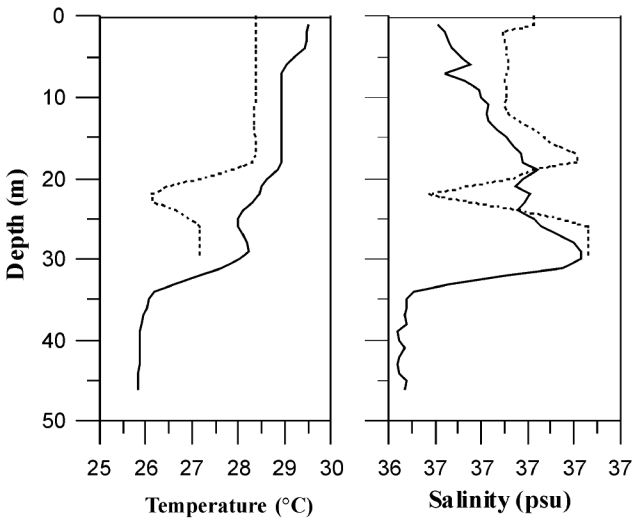


**Figure 2.** Initial temperature and salinity profiles used in internal wave simulator. Dashed line 7 May and solid line 8 May.

It can be seen from Figure 3 that all the variability in the measured profiles from top to bottom could not be reproduced by the model. However, a general level of sound speed variability could be reasonably well modelled, particularly in the thermocline region where IWs are present. From the measured and simulated sound speed variations, a covariance matrix[13,14] was constructed to compare the variance. The diagonal of the covariance matrix is the sound speed variance $\sigma^2$. Figure 4 shows variance as a function of depth for the two experiments. One finds that the sound speed variance calculated by IWAVE is in good agreement with the data, except near the surface on 7 May and between 25 and 30 m on 8 May 2002. Deviation at the surface layer on 7 May is due to other pheno-

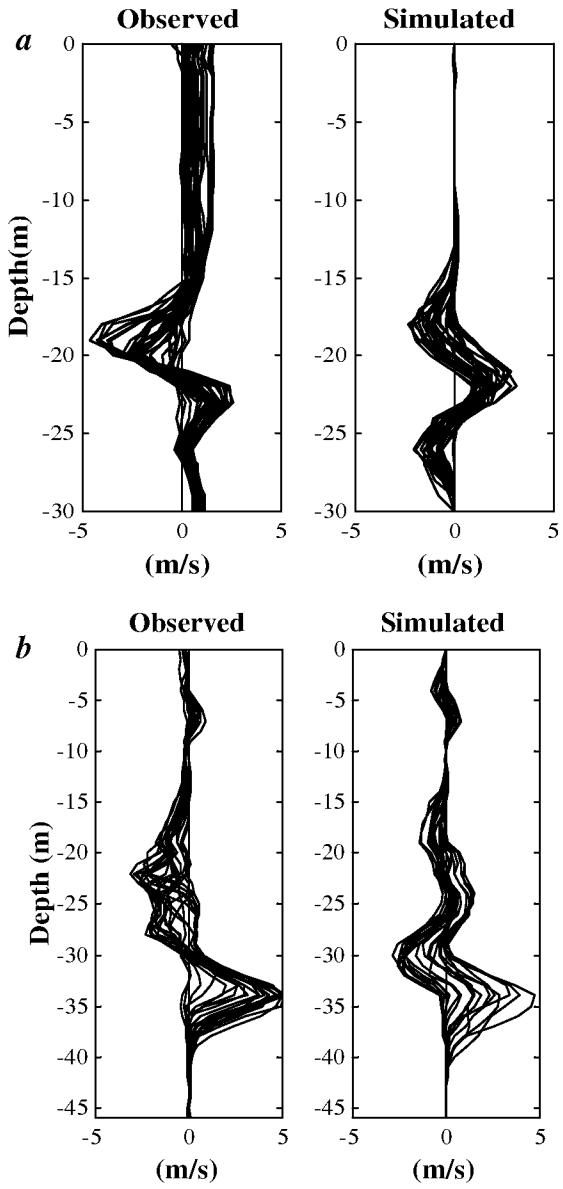


**Figure 3.** Comparison between measured and simulated sound speed perturbations for the CTD yo-yo experiment off Porbandar. (*a*) 7 May 2002 and (*b*) 8 May 2002.

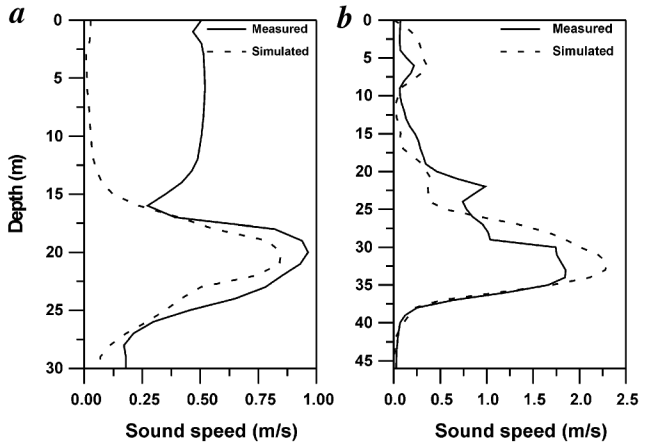


**Figure 4.** Measured and simulated sound speed variances. (*a*) 7 May 2002 and (*b*) 8 May 2002.

mena such as tides, etc. which are not included in the IWAVE. Deviations, particularly between 20 and 30 m on 8 May, are due to a sudden entrainment of cold and saline waters into the experimental site. This signal disappeared within the measurement time. Deviations could be attributed to the use of initial measured profile to initialize the model, since it does not contain any information as to the current state of the IW field (direction). Hence a simulation of the measurement period has an added uncertainty due to the use of random phases for each wave component.

An ocean simulation model for IW (IWAVE) was developed and validated against the measurements. A new technique was developed for calculation of dispersion relations, which is fast and stable. The model simulates the temperature and salinity structure due to IWs in the ocean. Comparisons between the measured and modelled variances of the sound speed are in good agreement. One of the main advantages of the IWAVE model is that it requires little information on the prevailing environment, but it serves as an effective and useful tool for understating the IW dynamics as well as the impact of these waves on underwater acoustic transmission. However, parameters such as $j_*$, $P$ and number of modes are site- and season-specific. Therefore, knowledge of these parameters at the experimental site improves the reliability of the simulated field. More experiments have to be conducted to validate and also to estimate parameters like $j_*$ and $P$ in the model, to improve its reliability.

1. Flatte, S. M. and Tappert, F. D., *J. Acoust. Soc. Am.*, 1975, **58**, 1151–1159.
2. Saunders, K. D. and King, D. B., In *Ocean Variability and Acoustic Propagation* (eds Potter, J. and Warn-Varnas, A.), Kluwer, 1991, pp. 561–577.
3. Colosi, J. A., Flatte, S. M. and Bracher, C., *J. Acoust. Soc. Am.*, 1994, **96**, 452–468.
4. Lynch, J. F. *et al.*, *J. Acoust. Soc. Am.*, 1996, **99**, 803–821.
5. Tielburger. D., Finette, S. and Wolf, S., *J. Acoust. Soc. Am.*, 1997, **101**, 789–808.
6. Gill, A. E., In *Atmosphere-Ocean Dynamics*, Academic Press, 1982.
7. Garrett, C. and Munk, W., *Geophys. Fluid Dyn.*, 1972, **2**, 225–264.
8. Garrett, C. and Munk, W., *J. Geophys. Res.*, 1975, **80**, 1321–1327.
9. Munk, W. H., In *Evolution of Physical Oceanography* (eds Warren, B. and Wunsch, C.), MIT Press, 1981, pp. 264–291.
10. Jackson, J. F. E. and Elliott, A. J., *Estuarine Coastal Shelf Sci.*, 2002, **54**, 51–64.
11. Elliott, A. J. and Jackson, J. F. E., In *IEEE Oceans'98*, 1998, pp. 10–14.
12. Krishna Kumar, G. V. and Balasubramanian, P., Departmental Research Report, 2004, 14/2004.
13. Yang, T. C. and Kwang Yoo., *IEEE J. Ocean Eng.*, 1999, **24**, 333–345.
14. Yang, T. C. and Kwang Yoo., In Proc. 8th Int. Congress Sound and Vibration, 2001, pp. 3001–3008.

ACKNOWLEDGEMENTS. We thank the Director, NPOL, Kochi for encouragement and support. We also thank all the participants of the field programme.

Received 27 September 2004; revised accepted 23 July 2005

# Three-phase tectonic evolution of the Andaman backarc basin

**K. A. Kamesh Raju**

National Institute of Oceanography, Dona Paula, Goa 403 004, India

**A three-phase evolutionary scheme since Late Oligocene for the Andaman backarc basin is proposed based on the multibeam swath bathymetry, magnetic and seismological data. A SW–NE trending spreading ridge bisects the basin. The tectonic evolution of the Andaman basin with special reference to the formation of oceanic crust within the backarc basin encompassing the backarc spreading, suggests a phase of ridge propagation. Swath bathymetry data documented topographic fabric of the ridge propagation and reveal several morphotectonic features that divide the basin into a complex western part comprising arc-parallel seamount chains, N–S trending fault systems and a relatively smooth eastern part. Spreading centre jump during Late Oligocene, rifting and extension during Middle Miocene to Early Pliocene followed by the recent true seafloor spreading since last 4 Ma define the three-phase tectonic evolution of the Andaman backarc basin. The recent phase has experienced westward propagation of**

e-mail: kamesh@darya.nio.org